# Supporting Information

**Capturing a *bis*-Fe(IV) state in *Methylosinus trichosporium* OB3b MbnH**

Anastasia C. Manesis*‡, Jeffrey W. Slater§, Kenny Cantave*, J. Martin Bollinger, Jr.§, Carsten Krebs§, and Amy C. Rosenzweig‡

*Departments of Molecular Biosciences and of Chemistry, Northwestern University, Evanston, IL 60208 USA.

§ Department of Chemistry and Department of Biochemistry and Molecular Biology, The Pennsylvania State University, University Park, Pennsylvania 16802 USA

‡Email : anastasia.manesis@northwestern.edu

## Table of Contents

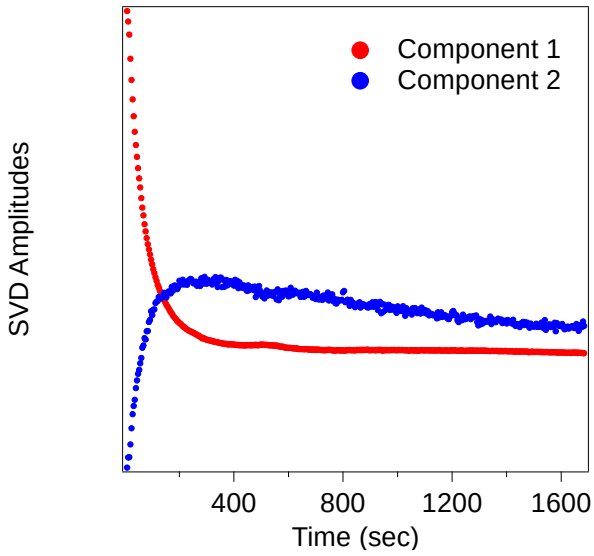


**Figure S1. Singular value decomposition analysis of time-resolved optical spectra in the nIR region following addition of 10 equivalents of $H_2O_2$ to MbnH.** Shown is the abstract component of two eigenvectors instead of one. The second eigenvector is primarily a noise vector as evidenced by its low significance value (0.618) and low autocorrelation coefficient (1.03).

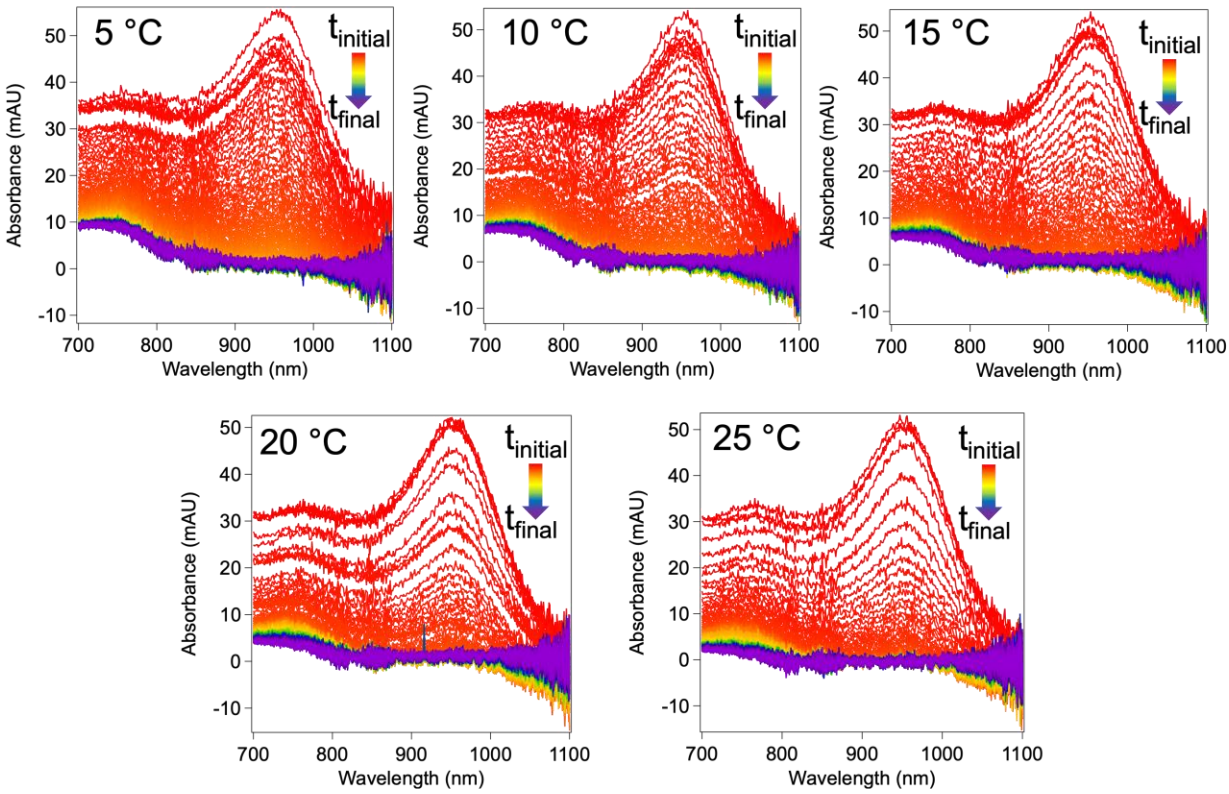


**Figure S2. Temperature dependence of the nIR feature of MbnH upon reaction with $H_2O_2$.** Decay of the nIR feature as a function of temperature upon mixing 200 μM $H_2O_2$ with 20 μM MbnH. Traces were collected every 4 sec for a total of 30 min.

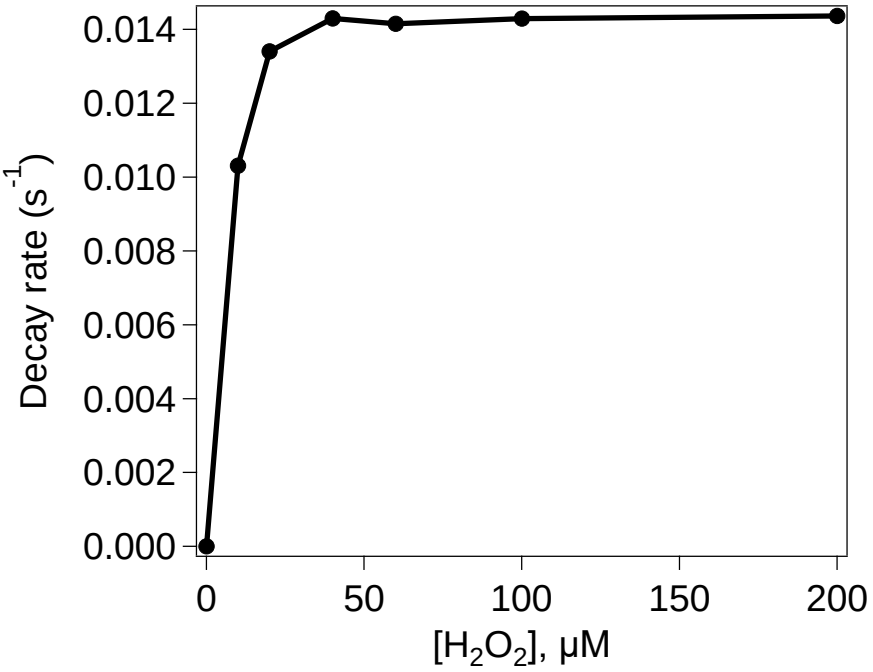


**Figure S3. Decay kinetics of MbnH reaction with $H_2O_2$.** Decay kinetics of the high-valent state monitored at 950 nm following the addition of $H_2O_2$ to 20 μM MbnH plotted as a function of $H_2O_2$ concentration.

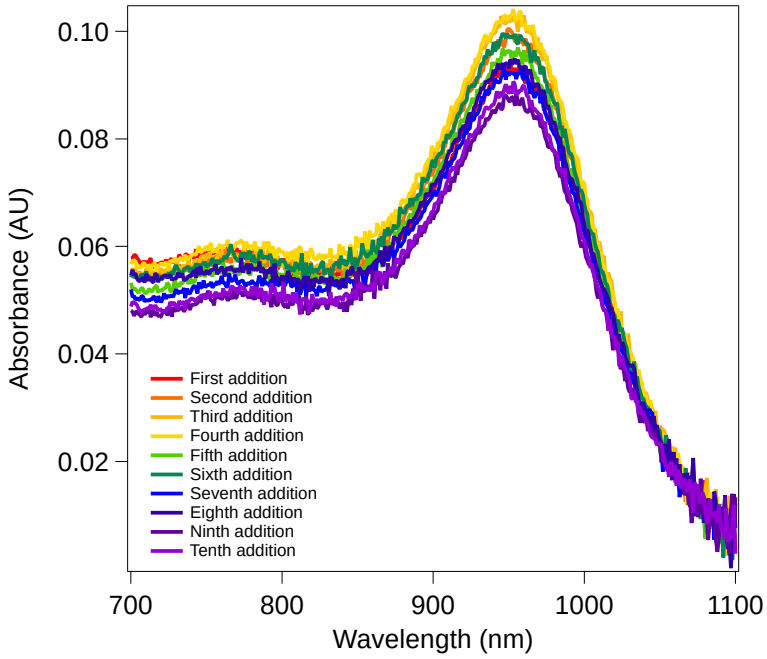


**Figure S4. Repeated reaction of MbnH with $H_2O_2$ monitored by formation of the 955 nm feature attributed to the *bis*-Fe(IV) state.** A spectrum was collected immediately following the addition of 200 μM $H_2O_2$ to ~20 μM MbnH (first addition, red trace), and spectra were collected every 4 sec for 30 min until the *bis*-Fe(IV) species decayed completed to the product state (spectra not shown). Another aliquot of 200 μM $H_2O_2$ was then added to the same sample, a spectrum was collected immediately (second addition, dark orange trace), and spectra were collected for another 30 min until the feature decayed completely (spectra not shown). This procedure was repeated 8 more times for a total of 10 additions.

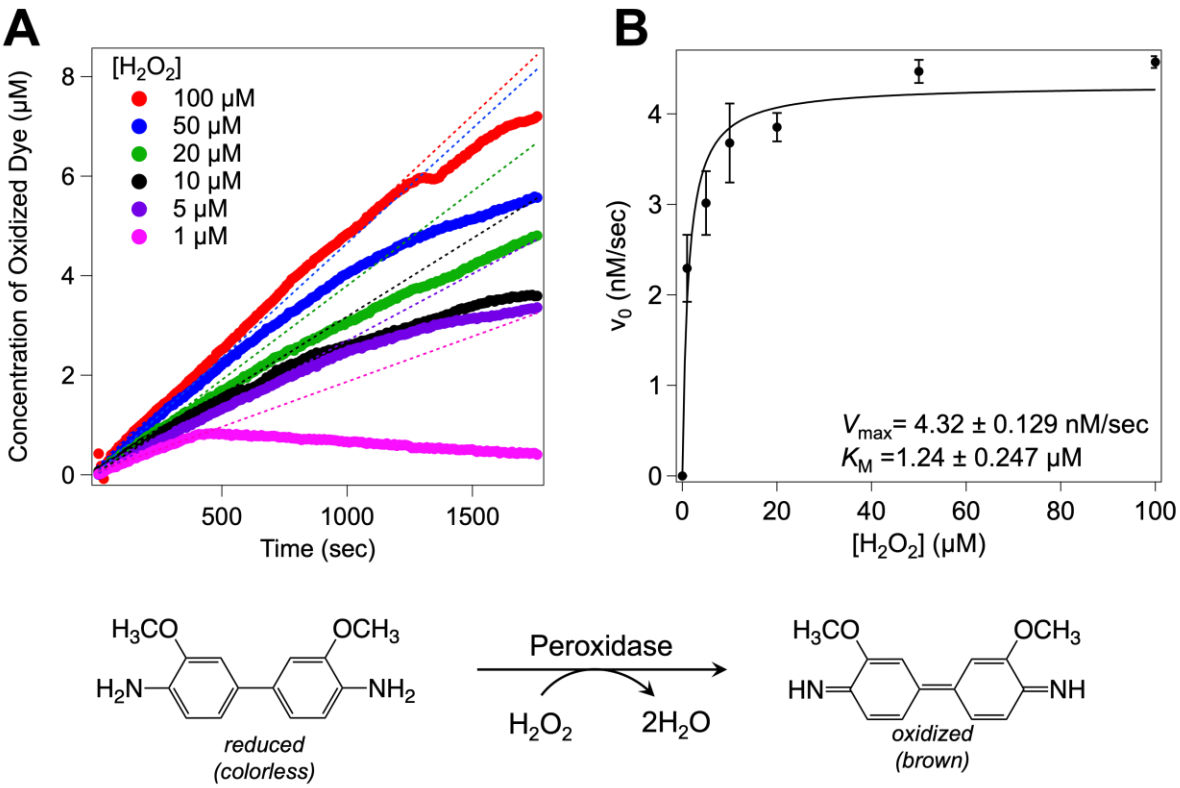


**Figure S5. MbnH dye-linked peroxidase assay.** (*A*) Kinetic traces monitoring the reaction of 20 nM MbnH with varying amounts of $H_2O_2$ in the presence of 100 µM *o*-dianisidine in 25 mM Tris, pH 7.2, 100 mM NaCl. Absorbance was monitored at 460 nm to track the gradual oxidation of the dye. The method of initial slopes was used to determine the initial reaction velocity. (*B*) Michaelis-Menten fit of the data averaged across three independent assays.

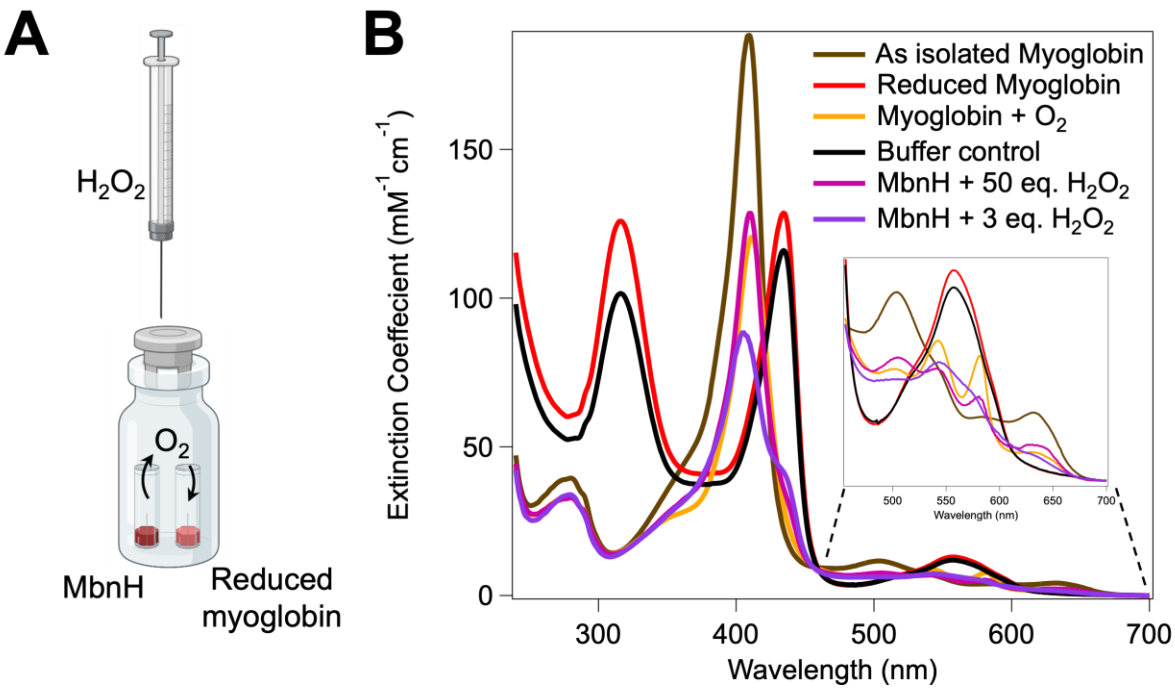


**Figure S6. MbnH myoglobin-linked assay.** (*A*) Diagram of assay setup. Reduced myoglobin and MbnH were placed in two separate vials within a septum-capped vial. $H_2O_2$ was added anaerobically to the MbnH vial, and each reaction vial was allowed to stir at room temperature for one hour. (*B*) UV-Vis spectra of myoglobin following the reaction of 300 μM MbnH with either 3 equivalents or 50 equivalents of $H_2O_2$ in 25 mM Tris, pH 7.2, 100 mM NaCl. Reduced myoglobin was used as a readout for oxygen production.

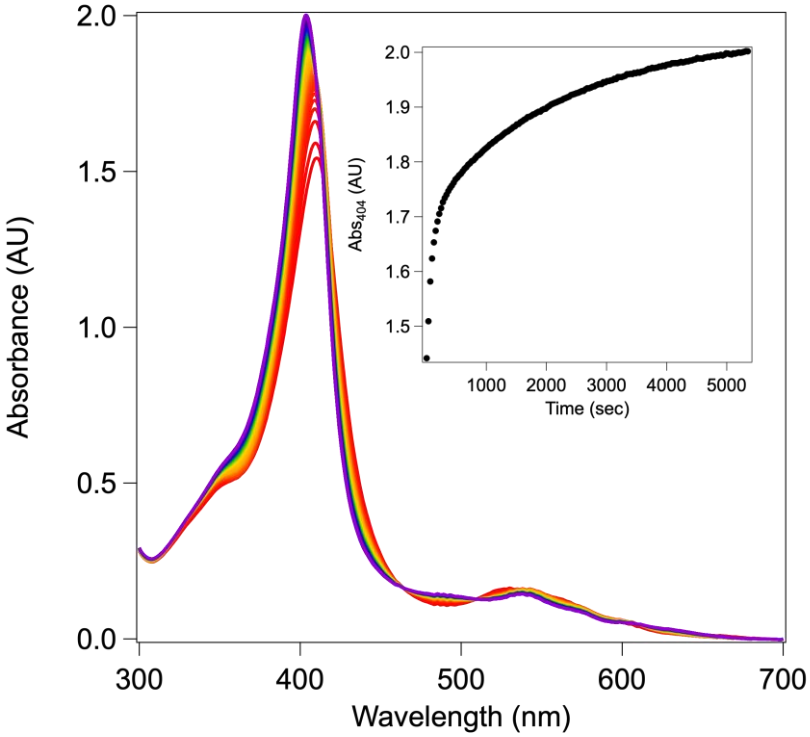


**Figure S7. Changes in the MbnH Soret band at 404 nm upon the addition of $H_2O_2$.** Spectra were collected immediately following the addition of 100 μM $H_2O_2$ to ~10 μM MbnH, and traces were collected every 30 sec for 3 hr. Inset shows the change in absorbance at 404 nm as a function of time.

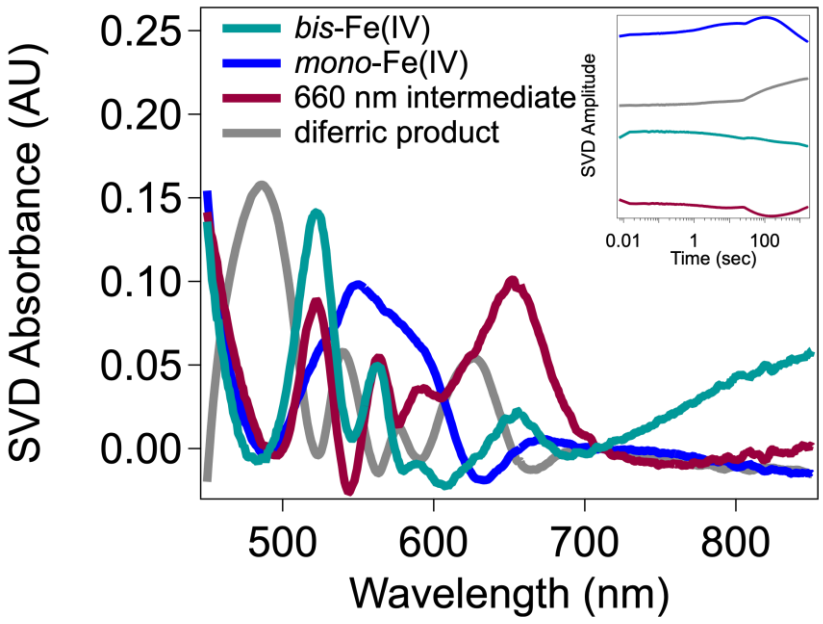


**Figure S8. Singular value decomposition analysis (SVD) analysis following the reaction of MbnH with $H_2O_2$.** Singular value decomposition of the Q-band region following the mixing of 200 μM $H_2O_2$ into 20 μM MbnH in a 1:1 ratio for 30 min. The SVD reveals four distinct components. Inset shows the SVD amplitudes for each identified component as a function of time.

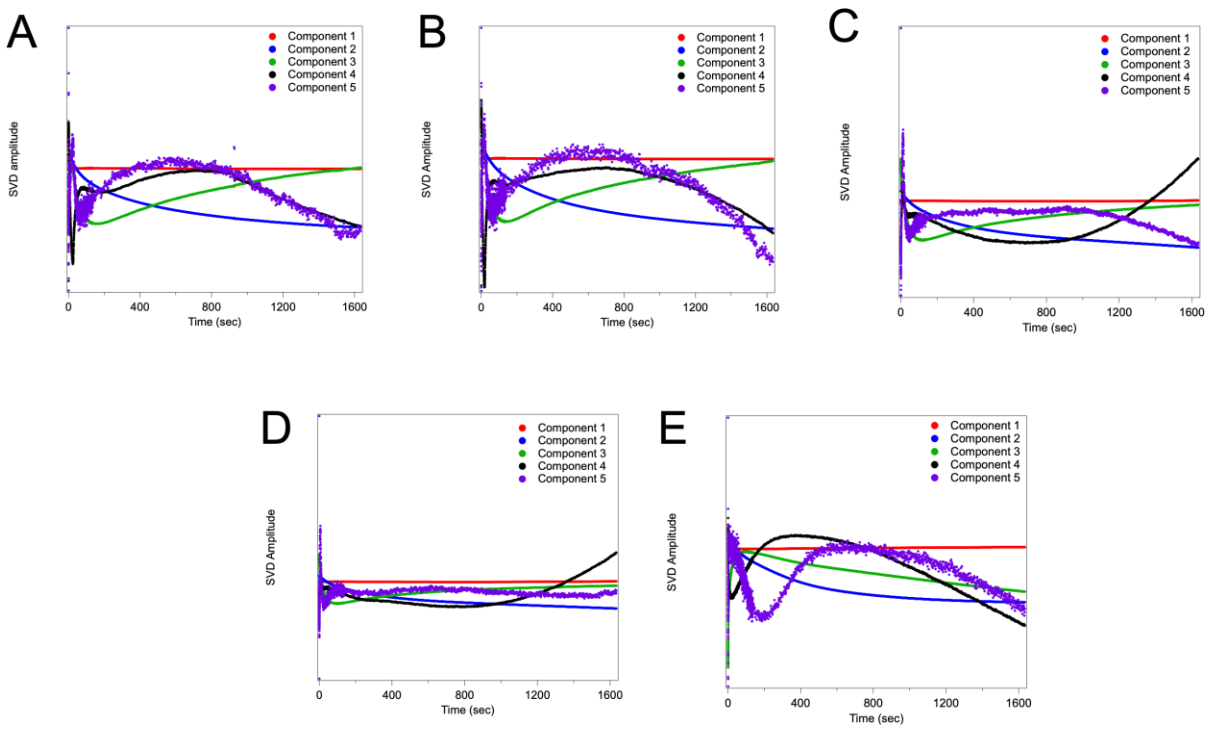


**Figure S9. SVD analysis of time-resolved optical spectra following addition of $H_2O_2$ to MbnH.** Deconvolution of spectra showing the abstract component of five eigenvectors instead of four at (*A*) 5 °C, (*B*) 10 °C, (*C*) 15 °C, (*D*) 20 °C, and (*E*) 25 °C. The fifth eigenvector is primarily a noise vector as evidenced by its low significance value and low autocorrelation coefficient.

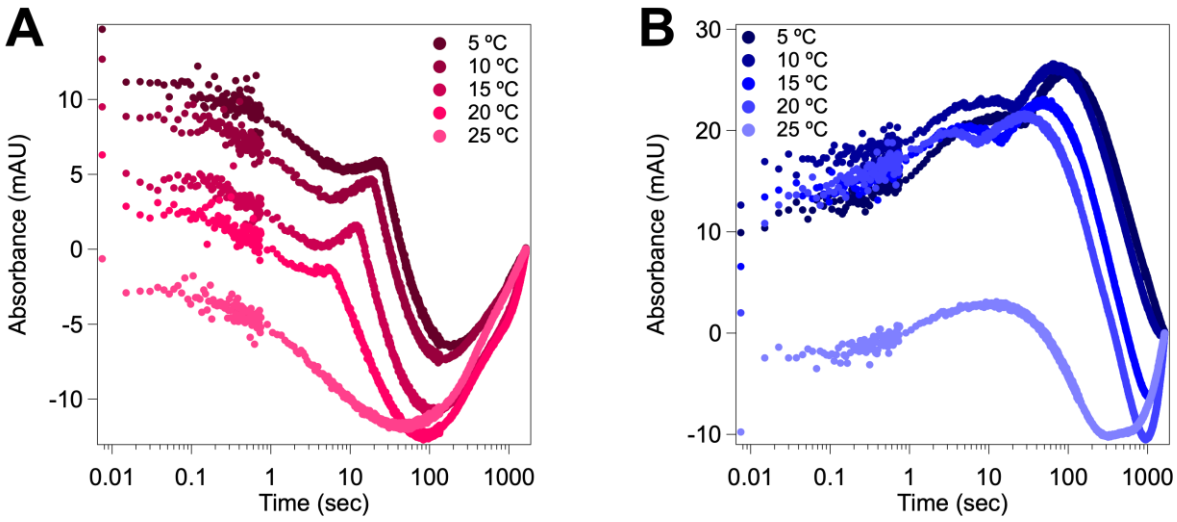


**Figure S10. Temperature dependence of the 660 nm and *mono*-Fe(IV) intermediates.** (*A*) Decay of the 660 nm feature at different temperatures. (*B)* Decay of the 555 nm feature at different temperatures.

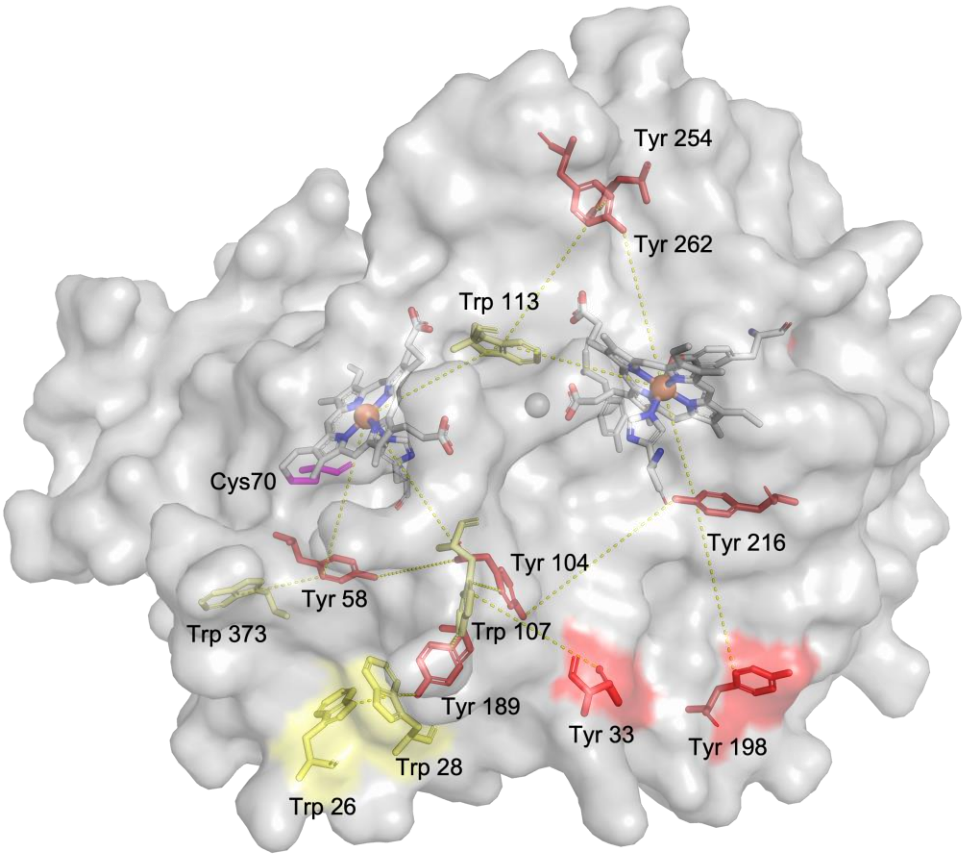


**Figure S11. Possible amino acid pathways that lead from the diheme cofactor to the surface.** Possible pathways composed of tryptophans (yellow) and tyrosines (red) that may serve to move an oxidizing equivalent from the diheme cofactor to the surface of the protein. All distances shown are less than 14 Å. Cys 70 (magenta) is another possible location for a protein-based radical.

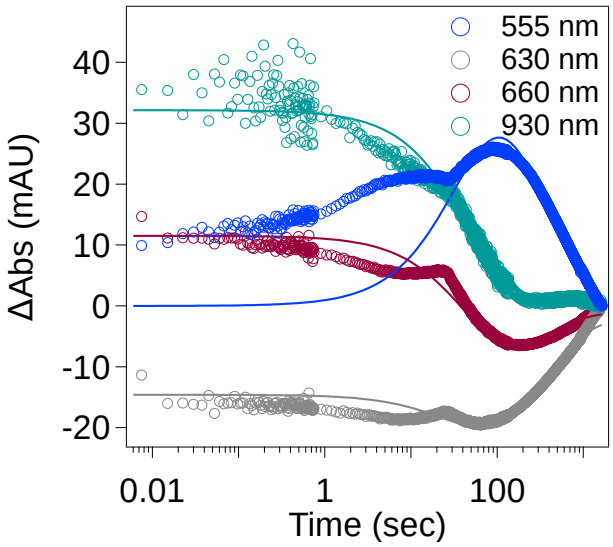


**Figure S12. Analysis of the decay kinetics of MbnH upon reaction with $H_2O_2$.** The kinetic traces (open circles) overlaid with the fit to the proposed model (lines) at wavelengths corresponding to *bis*-Fe(IV) (930 nm), $1e^-$ oxidized cofactor intermediate (555 nm), 660 intermediate (660 nm), and diferric product MbnH (630 nm) monitored at 5 °C using stopped-flow absorption spectroscopy. Spectra were collected immediately following mixing of 200 μM of peroxide with 20 μM MbnH in a 1:1 volume ratio for 30 min. The absorbance at 930 nm was used as a proxy for the 955 nm nIR feature.

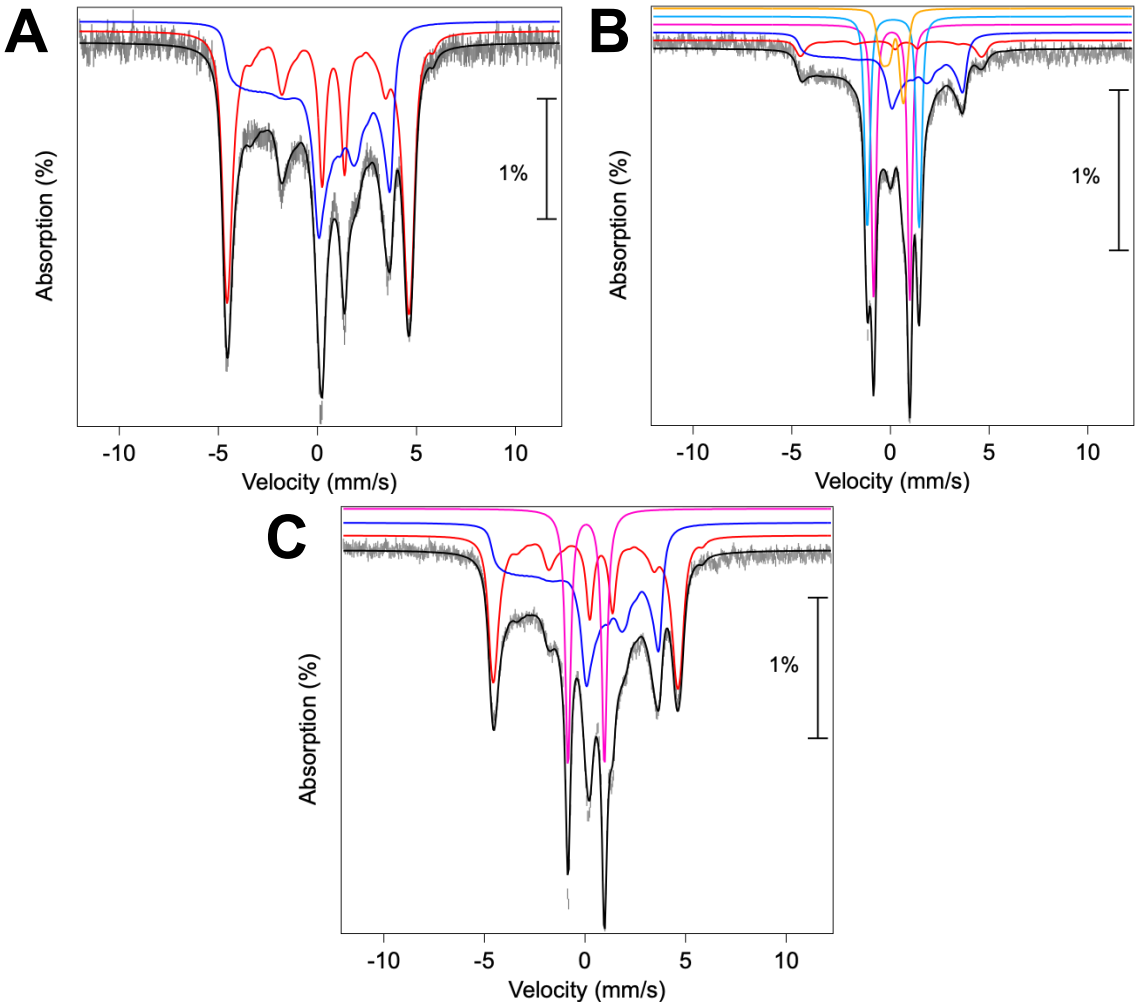


**Figure S13. Mössbauer spectra, recorded at 4.2 K in a 53 mT magnetic field applied parallel to the propagation of the $\gamma$-beam, of hand-quenched and rapid freeze-quenched samples from the reaction of diferric MbnH with $H_2O_2$.** (*A*) Spectra of diferric resting state MbnH and (*B*) MbnH reacted with 10 equivalents of $H_2O_2$ for 100 ms or (*C*) 100 sec. Both resting state and 100 sec samples were hand-quenched while the 100 ms sample was rapid freeze-quenched. The experimental spectra are depicted by gray vertical bars reflecting the standard deviations of the absorption during spectral acquisition. The black solid lines depict the overall simulated spectra, and the colored lines are theoretical spectra illustrating the fractional contributions from HS Fe(III) heme 1 (red), LS Fe(III) heme 2 (blue), Fe(IV) intermediate from heme 1 (pink), Fe(IV)

intermediate from heme 2 (light blue), and a third intermediate (yellow), to the experimental spectra. Simulation parameters and relative areas of these spectra are provided in Table 1 and Table S2.

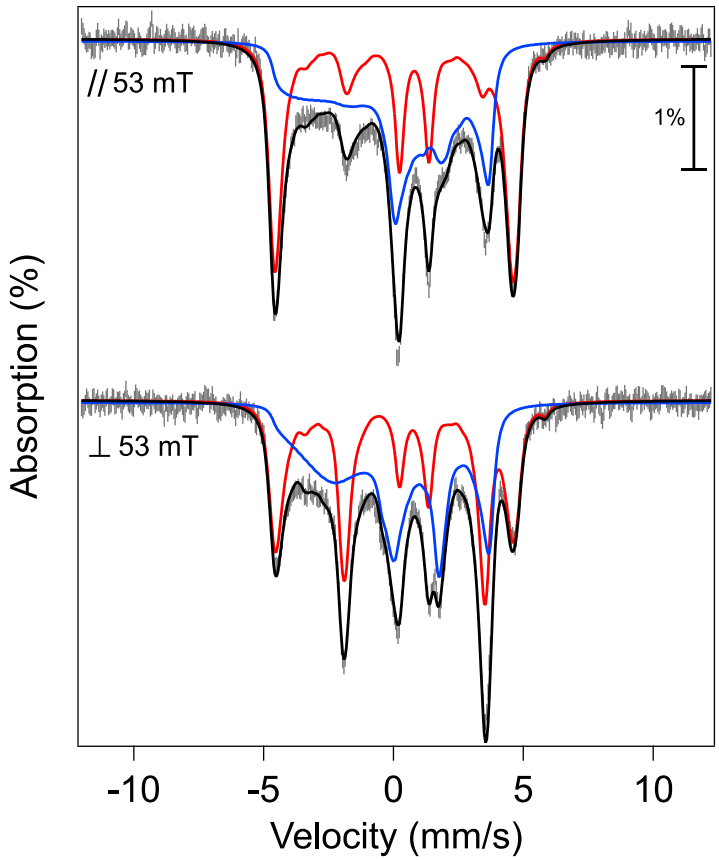


**Figure S14. Mössbauer spectra of diferric MbnH (gray bars) recorded at 4.2 K in a 53 mT magnetic field parallel (top) and perpendicular (bottom) to the $\gamma$-beam.** The Hamiltonian simulations of the LS Fe(III) heme (55% of total Fe, blue), HS Fe(III) heme (45% of total Fe, red), and the summation spectrum (black) are overlaid and simulated with the following parameters: S = 1/2, $g_{1/2}$ = (1.811, 2.234, 2.620), $\delta$ = 0.30 mm/s, $\Delta E_Q$ = 2.65 mm/s, $\eta$ = -2.3, $A/g_N\beta_N$ = (-452, 71, 288) kG and S = 5/2, $g_{5/2}$ = 2, $D_{5/2}$ = 5 $cm^{-1}$, $(E/D)_{5/2}$ = 0, $\delta$ = 0.42 mm/s, $\Delta E_Q$ = 1.68 mm/s, $\eta$ = -0.1, $A/g_N\beta_N$ = (-182, -194, -190) kG.

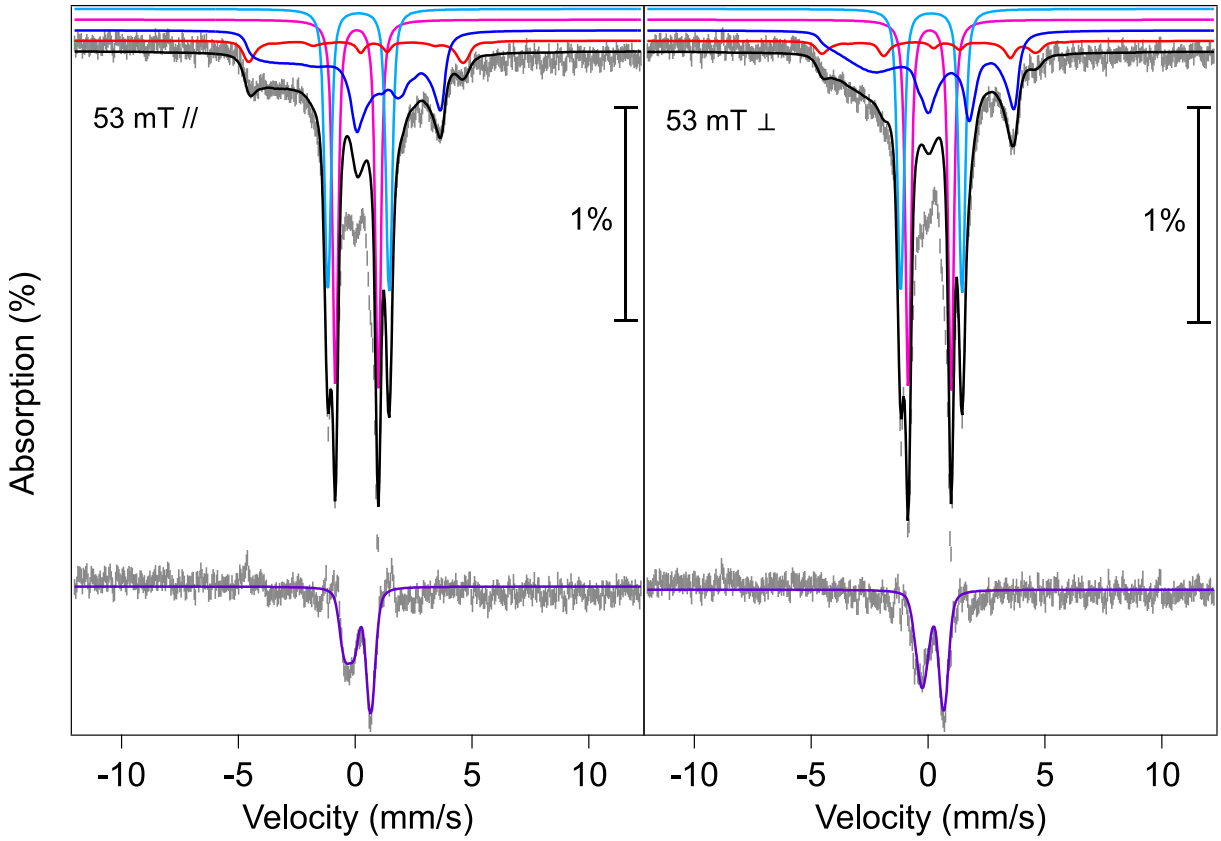


**Figure S15. Analysis of the 4.2-K Mössbauer spectra of the 100-ms sample collected in magnetic fields of 53 mT applied parallel (left panel) or perpendicular (right panel) to the propagation direction of the $\gamma$-beam**. In both panels, the raw data is depicted as gray vertical bars in the top spectra and the simulations of the four main components contained in the sample [high-spin Fe(III) heme 1 (red line), low-spin Fe(III) heme 2 (blue line), ferryl heme 1 (magenta), and Fe(IV) heme 2 (light blue)] using the parameters quoted in the main text and Table ST1 are shown as colored lines. The total contribution of these four components is shown as black solid line. Subtraction of these components reveals the features of the remaining component (~10% of total Fe), which appears as a quadrupole doublet with a significantly broader low-energy line (gray vertical bars, bottom spectra). This component was analyzed with the assumption that it might arise from cmpd-I of heme 1 for two reasons. First, the analysis of the stopped-flow absorption

data revealed a transient absorption band that is consistent with the assignment to cmpd-I. Second, cmpd-I from horseradish peroxidase (HRP-I) exhibits Mossbauer features that are qualitatively similar to those observed in MbnH, i.e. an apparent quadrupole doublet, of which the left line is broadened due to hyperfine interaction. In general, cmpd-I consists of a Fe(IV)=O heme center ($S_{Fe}$ = 1) with a large axial zero-field splitting tensor exchange-coupled to a radical on the porphyrin ring and/or the axial ligand ($S_{rad}$ = 1/2). The properties of the resulting three Kramers doublets strongly depend on the ratio $J/D_{Fe}$. HRP-1 exhibits a rather small J/D of ~0.1, resulting only in small spin expectation values of the heme site, and consequently only small hyperfine interactions that give rise to the weak but noticeable hyperfine broadening of the low-energy line of the quadrupole doublet. The fit of a spin Hamiltonian simulation to the reference spectra yields the following parameters (purple lines): $S_{Fe}$ = 1, $S_{rad}$ = 1/2, $D_{Fe}$ = 25 cm-1 (fixed), $(E/D)_{Fe}$ = 0 (fixed), $\mathbf{g}_{Fe}$ = 2.0 (fixed), $\mathbf{g}_{rad}$ = 2.0 (fixed), $J$ = 3 $cm^{-1}$ (fixed), $\delta$ = 0.20 mm/s, $\Delta E_Q$ = 0.88 mm/s , $\eta$ = 0 (fixed), $A/g_N\beta_N$ = (-25.0, -8.3, -7.6) T; the hyperfine and electric field gradient tensors were assumed to be collinear. We note that the isomer shift of 0.20 mm/s would be unusually high for the assignment of this component to cmpd-I. Likewise, the weak, but noticeable field-orientation dependence of the experimental and simulated spectra does not agree well with this assignment.

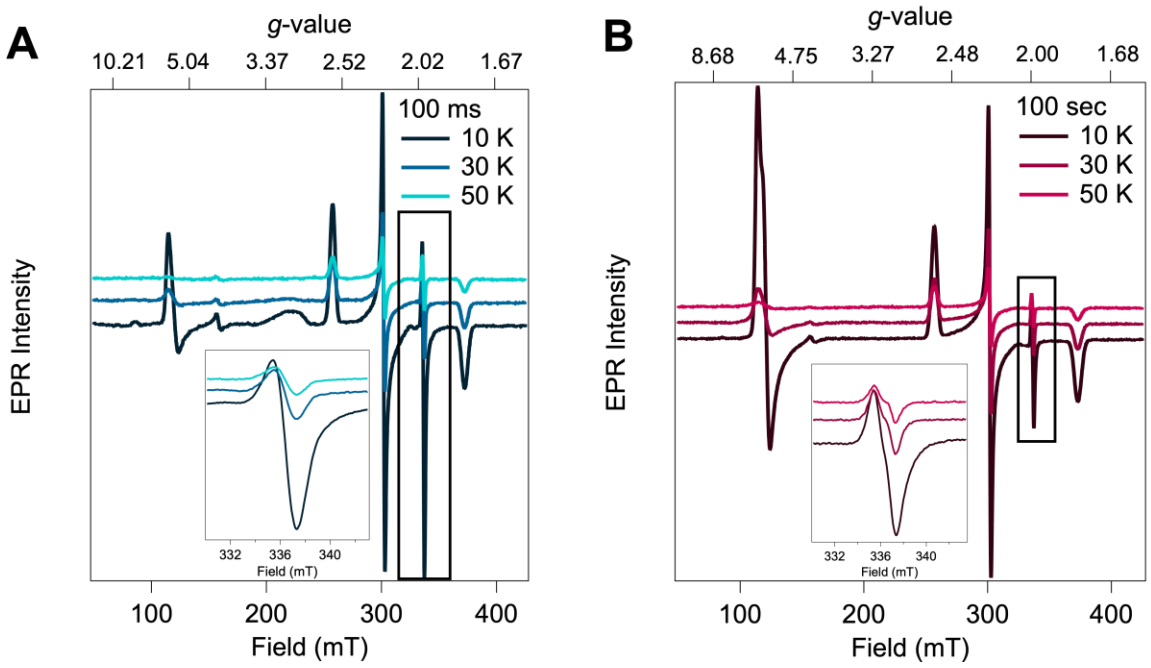


**Figure S16. CW EPR spectra as a function of temperature.** (*A*) Full CW-EPR field sweep of MbnH mixed with 10 equivalents of $H_2O_2$ and freeze-quenched at 100 ms. Spectra were recorded at temperatures of 10-50 K, microwave power of 0.1585 mW, modulation amplitude of 1 mT, and frequency of 9.43684 GHz. Inset shows a zoom in of the radical region. (*B*) Full CW-EPR field sweep of MbnH hand-mixed with 10 equivalents of $H_2O_2$ and hand-quenched at 100 sec. Spectra were recorded at temperatures of 10-50 K, microwave power of 0.1585 mW, modulation amplitude of 1 mT, and frequency of 9.43684 GHz. Inset shows a zoom in of the radical region.

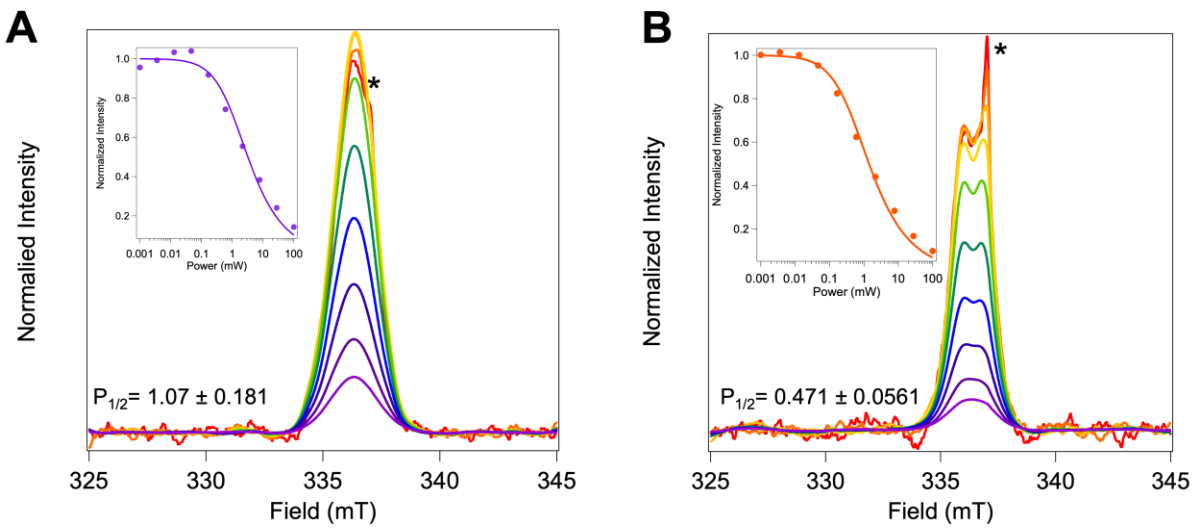


**Figure S17. CW EPR spectra as a function of power.** (*A)* CW-EPR field sweep of MbnH mixed with 10 equivalents of $H_2O_2$ and freeze-quenched at 100 ms. (*B)* CW-EPR field sweep of MbnH hand-mixed with 10 equivalents of $H_2O_2$ and hand-quenched at 100 sec. All spectra were recorded at 75 K, modulation amplitude of 0.2 mT, and a frequency of 9.43684 GHz. Insets shows the power saturation curve fitting the extracted maximum intensity at fields (A) 336.4 mT and (B) 336.0 mT to Equation 3. The sharp feature at $g$= 2.000 (starred feature) is attributed to an organic-based free radical signal.

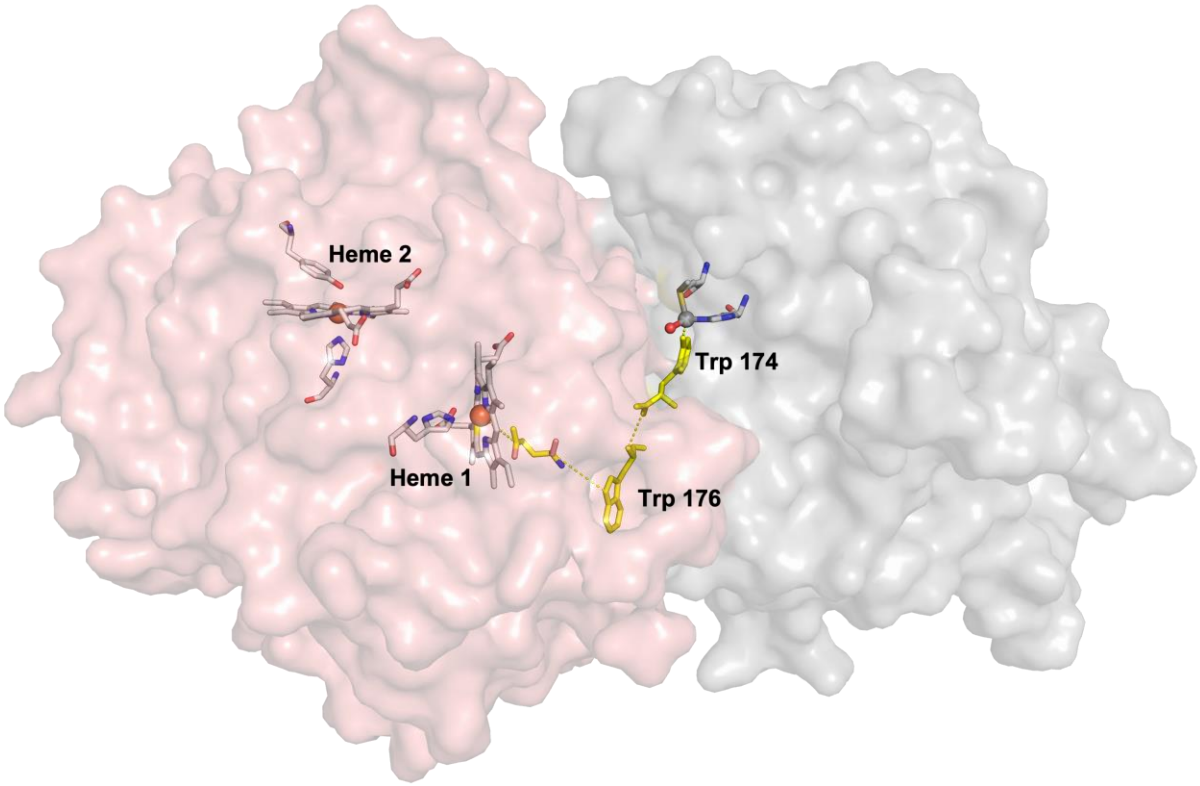


**Figure S18. Predicted MbnPH structure.** The structure of the MbnPH complex was predicted using Alphafold2. MbnH is shown in salmon and MbnP is shown in gray. Iron ions are shown as orange colored spheres, and the copper ion in MbnP is shown as a gray sphere with a coordinating solvent molecule as a red sphere. The residues involved in the electron transfer pathway between Trp174 of MbnP and heme 1 of MbnH predicted by HARLEM are shown in yellow.

**Table S1**. **Comparison of spectroscopic and redox properties of MbnH, MauG, and BthA**.

| | | **MbnH** [a, vide infra] | **MauG** [b, c, d] | **BthA** [e] |
|---|---|---|---|---|
| Fe(III)/Fe(II) Reduction Potentials (versus NHE at pH 7.5) | $E_{m1}$ | -38 ± 2 mV | –159 ± 10 mV | – 121 mV |
| | $E_{m2}$ | – 257 ± 5 mV | – 244 ± 5 mV | -165 mV |
| Mossbauer Parameters for *bis*-Fe(IV) | Heme-1 | δ = 0.06 mm/s<br>ΔEq = 1.81 mm/s | δ = 0.06 mm/s<br>ΔEq = 1.70 mm/s | δ = 0.07 mm/s<br>ΔEq = 1.70 mm/s |
| | Heme-2 | δ = 0.13 mm/s<br>ΔEq = 2.63 mm/s | δ = 0.17 mm/s<br>ΔEq = 2.54 mm/s | δ = 0.17 mm/s<br>ΔEq = 2.58 mm/s |
| *g*-values$_{diferric}$ | High spin heme-1 | $g_{\parallel}$ = 1.99<br>$g_{\perp}$ = 5.61 | $g_{\parallel} \approx$ 1.99<br>$g_{\perp} \approx$ 5.57 | $g_{\parallel} \approx$ 2<br>$g_{\perp} \approx$ 6 |
| | Low-spin heme-2 | $g_1$ = 1.81<br>$g_2$ = 2.23<br>$g_3$ = 2.62 | $g_1 \approx$ 1.87<br>$g_2 \approx$ 2.19<br>$g_3 \approx$ 2.54 | $g_1$ = 1.86<br>$g_2$ = 2.19<br>$g_3$ = 2.54 |
| $Abs_{Soret\ (diferric)}$ | | 404 nm | 406 nm | 403 nm |
| Peroxidase Activity | $k_{cat}$ | 0.22 $s^{-1}$ | 1.06 $s^{-1}$ | 5.44 $s^{-1}$ |
| | $K_M$ | 1.24 ± 0.25 μM | N.R | 3.4 ± 0.4 μM |

[a] Kenney, G. E.; Dassama, L. M. K.; Manesis, A. C.; Chen, S.; Ross, M. O.; Hoffman, B. M.; Rosenzweig, A. C. *J. Biol. Chem*. **2019**

[b] Li, X.; Feng, M.; Wang, Y.; Tachikawa, H.; Davidson, V. L. *Biochemistry* **2006**, 45, 821–828

[c] Li, X.; Fu, R.; Lee, S.; Krebs, C.; Davidson, V. L.; Liu, A. *Proc. Natl. Acad. Sci*. **2008**, 105, 8597–8600

[d] Wang, Y.; Graichen, M. E.; Liu, A.; Pearson, A. R.; Wilmot, C. M.; Davidson, V. L. *Biochemistry* **2003**, 42, 7318–7325

[e] Rizzolo, K.; Cohen, S. E.; Weitz, A. C.; Muñoz, M. M. L.; Hendrich, M. P.; Drennan, C. L.; Elliott, S. J. *Nat. Commun*. **2019**, 10, 1101

**Table S2**. **Relative intensity of Mössbauer subspectra**.

| | **Diferric (0s)** | **100 ms** | **100 s** |
|---|---|---|---|
| HS Heme 1 Fe(III) | 45% | 5% | 26% |
| Heme 1 Fe(IV) | 0% | 26% | 18% |
| **Heme 1 Total** | **45%** | **31%** | **44%** |
| LS Heme 2 Fe(III) | 55% | 35% | 56% |
| Heme 2 Fe(IV) | 0% | 20% | 0 % |
| **Heme 2 Total** | **55%** | **55%** | **56%** |
| 3rd intermediate | 0% | 14% | 0% |

The estimated uncertainty for the area of subspectra is ~3% for quadrupole doublets and ~5% for magnetically split subspectra.